Data in Brief 21 (2018) 1375–1380

Contents lists available at ScienceDirect

Data in Brief

journal homepage: www.elsevier.com/locate/dib

Data Article

Anisotropy and directional elastic behavior data obtained from the second-order elastic constants of portlandite $Ca(OH)_2$ and brucite $Mg(OH)_2$

Gianfranco Ulian, Giovanni Valdrè *

Dipartimento di Scienze Biologiche, Geologiche e Ambientali, Centro di Ricerche Interdisciplinari di Biomineralogia, Cristallografia e Biomateriali, Università di Bologna "Alma Mater Studiorum", Piazza di Porta San Donato 1, 40126 Bologna, Italy

ARTICLE INFO

Article history:
Received 12 July 2018
Received in revised form
23 October 2018
Accepted 26 October 2018
Available online 30 October 2018

ABSTRACT

This article reports data on the anisotropy and directional elastic behavior, namely Young's modulus E, linear compressibility β, shear modulus μ, Poisson's ratio ν and wave velocities V_{s1}, V_{s2} and V_p, of brucite (magnesium hydroxide, $Mg(OH)_2$) and portlandite (calcium hydroxide, $Ca(OH)_2$), calculated from their second order elastic constants at different hydrostatic compressions (Ulian and Valdrè, in press). The dataset has been obtained by *ab initio* quantum mechanical means, by employing density functional theory methods, in particular the B3LYP hybrid functional, all-electron Gaussian-type orbitals basis sets and a correction to take into account the effects of dispersive forces.

© 2018 The Authors. Published by Elsevier Inc. This is an open access article under the CC BY-NC-ND license (http://creativecommons.org/licenses/by-nc-nd/4.0/).

Specifications table

Subject area	*Physics*
More specific subject area	*Directional mechanical properties of hydroxyl mineral structures calculated from their second order elastic constants at different pressures*
Type of data	*Table and figure*

* Corresponding author.
E-mail address: giovanni.valdre@unibo.it (G. Valdrè).

https://doi.org/10.1016/j.dib.2018.10.139
2352-3409/© 2018 The Authors. Published by Elsevier Inc. This is an open access article under the CC BY-NC-ND license (http://creativecommons.org/licenses/by-nc-nd/4.0/).

How data were acquired	*Quantum mechanical simulations at the DFT/B3LYP level of theory, including dispersive forces contributions (CRYSTAL14 code)*
Data format	*Raw, analyzed*
Experimental factors	*Initial geometries were taken from experimental data available in literature*
Experimental features	*Quantum mechanical simulations conducted using Density Functional Theory, B3LYP functional and Gaussian-type orbitals basis sets.* *Inclusion of dispersive forces contribution via DFT-D2 scheme, corrected for the B3LYP functional (B3LYP-D* approach).* *Unit cell under different hydrostatic compression states.*
Data source location	*Bologna, P. Porta San Donato 1, Italy*
Data accessibility	*Data are displayed within this article.*
Related research article	*This Data in Brief article is related to the paper:* *Ulian, G. & Valdrè, G. (2018) Equation of state and second-order elastic constants of portlandite $Ca(OH)_2$ and brucite $Mg(OH)_2$. Physics and Chemistry of Minerals, in press,* doi:10.1007/s00269-018-0989-3.

Value of the data

- Elastic constants and related properties of brucite (magnesium hydroxide, $Mg(OH)_2$) and portlandite (calcium hydroxide, $Ca(OH)_2$) in space group settings $P\bar{3}m1$ and $P\bar{3}$, useful for mechanical applications of these mineral phases.
- Data obtained at the density functional theory (DFT) level, employing hybrid B3LYP functional and including a correction to take into account the contribution of dispersive forces, which could be useful for *ab initio* comparisons of similar materials.
- The present data could be helpful for researchers involved in the mechanical properties of hydroxyl phases under the effect of applied pressure, *e.g.* for geological and building/cement applications.

1. Data

1.1. Brucite and portlandite mechanical properties variations with direction

Single-crystal elastic properties of both brucite and portlandite were calculated at $T = 0$ in the Cartesian space by using the second order elastic constants obtained in a previous work [1]. Two space group settings were considered, namely $P\bar{3}m1$, where the hydroxyl groups are all oriented along the [001] direction and $P\bar{3}$, which included some proton disorder in the structure. The effect of weak van der Waals interactions in both the equilibrium and hydrostatically compressed unit cells, and thus on the mechanical properties, was also taken into account. This is an important topic for both the mechanical and the surface properties for layered minerals. For the sake of clearness, in Table 1 the unit cell volumes of brucite and portlandite in each symmetry setup and their corresponding pressure are reported [1].

Overall, the directional Young's modulus E, linear compressibility β, shear modulus μ, Poisson's ratio ν and wave velocities V_{s1}, V_{s2} and V_p were calculated on the (xy), (xz) and (yz) planes for 44 structures and are reported in the Supplementary materials as follows:

- Brucite (s.g $P\bar{3}m1$) – Tables S1–11;
- Brucite (s.g $P\bar{3}$) – Tables S12–22;
- Portlandite (s.g $P\bar{3}m1$) – Tables S23–33;
- Portlandite (s.g $P\bar{3}$) – Tables S34–44.

Table 1
Simulated unit cell volumes and the corresponding pressure values of brucite and portlandite in the space group settings $P\bar{3}m1$ and $P\bar{3}$.

Model	Brucite $P\bar{3}m1$		Brucite $P\bar{3}$		Portlandite $P\bar{3}m1$		Portlandite $P\bar{3}$	
	P (GPa)	V (Å^3)	P (GPa)	V (Å^3)	P (GPa)	V (Å^3)	P (GPa)	V (Å^3)
P01	−1.99	41.9998	−1.73	124.4219	−1.29	57.2331	−1.15	169.236
P02	−1.35	41.0678	−1.37	122.6337	−0.80	55.9663	−0.90	167.5269
P03	−0.51	40.1503	−0.63	120.0533	−0.20	54.7127	−0.43	164.5618
P00	0.08	39.6302	−0.04	118.4413	0.05	54.0043	−0.06	161.8418
P04	0.58	39.2426	0.48	117.3462	0.54	53.4761	0.26	160.1480
P05	1.95	38.3476	1.94	114.5878	1.43	52.2556	1.15	156.3257
P06	3.65	37.4628	3.75	111.8689	2.49	51.0434	2.24	152.6057
P07	5.71	36.5942	5.87	109.2402	3.76	49.8562	3.52	149.0702
P08	8.20	35.7381	8.30	106.7016	5.24	48.6894	4.96	145.7070
P09	11.19	34.8928	11.03	104.2052	6.97	47.5477	6.57	142.4289
P10	14.67	34.0735	14.00	101.8082	8.96	46.4321	8.34	139.228

The reported data can be employed, for instance, to create polar plots of the desired quantities and compare them to other theoretical or experimental results. An example of this application is reported in Fig. 1.

2. Experimental design, materials, and methods

The data here presented were calculated from the results obtained by first principle simulations on periodic systems, using both the CRYSTAL14 [2] and CRYSTAL17 codes [3], which implements the Hartree–Fock and Kohn–Sham self-consistent field method. The same approach was employed to investigate the elastic behaviour of other phases containing hydroxyl groups [4].

2.1. Basis set

Multi-electron wave functions are constructed as an antisymmetrized product (Slater determinant) of monoelectronic crystalline orbitals (CO) that are linear combination of local functions (atomic orbitals, AO) centred on each atom in the system. In turn, atomic orbitals (basis set) are linear combinations of Gaussian-type functions (GTF). The all-electron basis sets employed in the present simulations for Ca^{2+} and Mg^{2+} were a 86–511 G* and a 8–511 G* basis sets [5–9]. For O and H atoms, a triple-ζ basis set with polarization from to the work of Ahlrichs and co-workers [10] has been adopted for both atoms.

2.2. Hamiltonian and computational parameters

The Becke [11] three-parameter (B3LYP) hybrid exchange functional in combination with the gradient-corrected correlation functional of Lee et al. [12] has been adopted for all calculations.The exchange–correlation contribution is performed over a grid of points and is the result of a numerical integration of the electron density and its gradient. The adopted pruned grid is given by 75 points and 974 angular points (XLGRID) and obtained from The Gauss–Legendre quadrature and Lebedev schemes [13]. The tolerance thresholds that control accuracy of the Coulomb and exchange integrals were set to 10^{-7} and 10^{-16}, respectively [2]. The Hamiltonian matrix has been diagonalized using a Monkhorst grid of k-points of size $8 \times 8 \times 8$ for the high symmetry models (s.g. $P\bar{3}m1$), whereas a $4 \times 4 \times 4$ grid was employed for the low symmetry (s.g. $P\bar{3}$) ones.The convergence on total energy was reached when the difference between the energy of two subsequent self-consistent field cycles was less than 10^{-8} Ha.

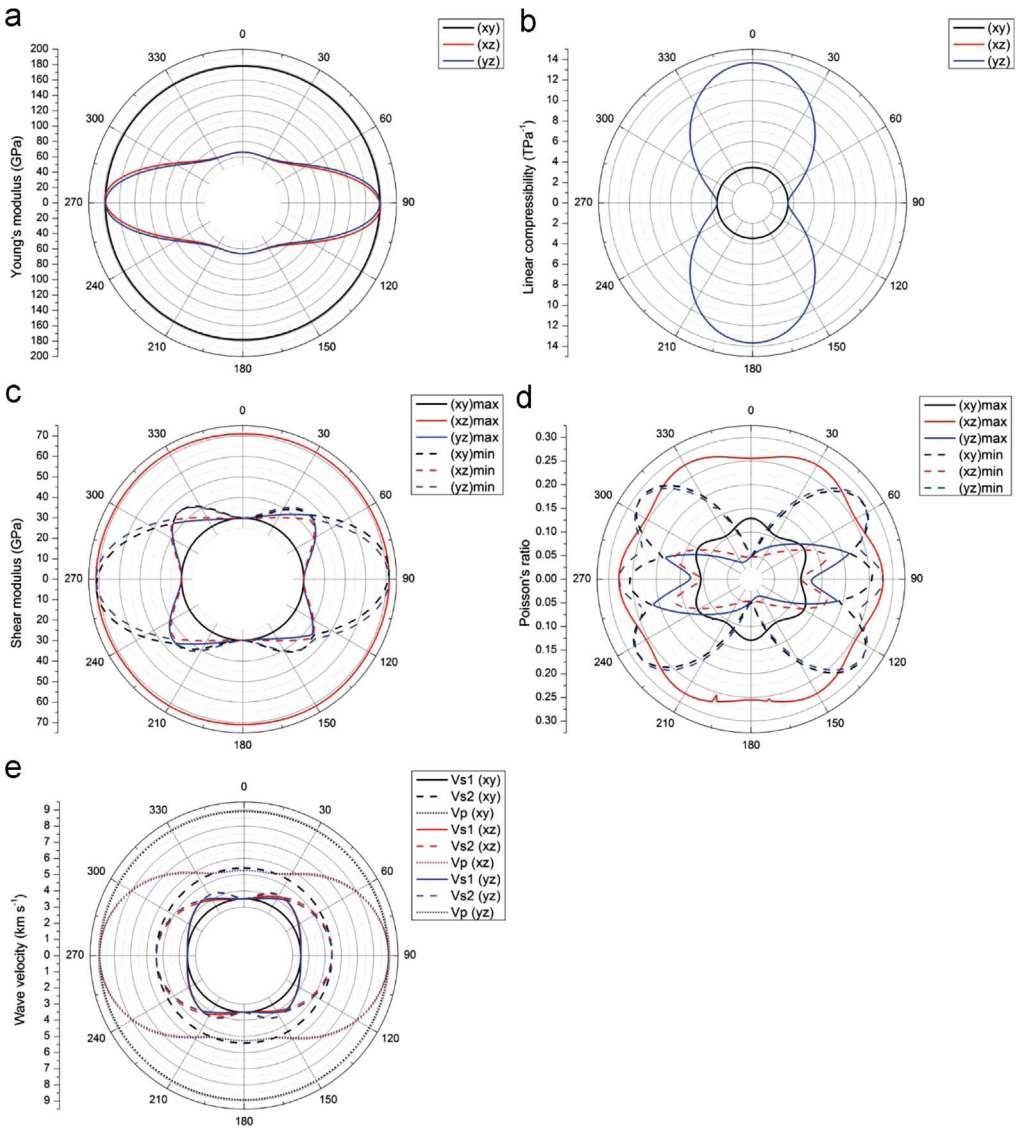

Fig. 1. Directional dependence of Young's modulus E (a), linear compressibility β(b), shear modulus μ (c), Poisson's ratio ν (d) and wave velocities V_{s1}, V_{s2} and V_p on the (x,y), (x,z) and (y,z) planes, for brucite model P00 (s.g. $P\bar{3}m1$, pressure 0.08 GPa). In (c,d) plots, solid lines are referred to the maximum values and dashed ones to the minimum ones.

Van der Waals (dispersive) forces were included with the (DFT+D2 scheme [14], which adds the following contribution to the calculated DFT energy:

$$E_{DISP} = -s_6 \sum_{\mathbf{g}} \sum_{i \neq j} f_{dump}\left(R^6_{ij.\mathbf{g}}\right) \frac{C_6^i C_6^j}{R^6_{ij.\mathbf{g}}} \tag{1}$$

The summation over all atom pairs ij and g lattice vectors excludes the self-interaction contribution ($i = j$) for every g. The parameters ${C_6}^i$ represent the dispersion coefficient for the atom i, $R_{ij.\mathbf{g}}$ is the interatomic distance between atom i in the reference cell and atom j in the neighbouring cells at distance |g| and s_6 is a functional-dependent scaling factor. The function f_{dump} is used to dump the

energy correction to avoid double counting of short-range contributions to the energy and depends on the sum of atomic van der Waals radii and on a steepness parameter ($d = 20$). Due to the molecular nature of the DFT+D2 scheme, which tends to overestimate cohesive energy in solid crystals, the original B3LYP+D parameters where modified, setting s_6 to 1, R_{vdw}(H) to 1.30 and the heavier atom van der Waals radii were scaled by a factor 1.05 (B3LYP-D* approach) [15–17].

2.3. Calculation of directional elastic properties

For the calculation of the directional dependence of the cited elastic properties, the stiffness tensor was transformed by means of:

$$T'_{\alpha\beta\gamma\delta} = r_{\alpha i} r_{\alpha i} r_{\alpha i} r_{\alpha i} T_{ijkl} \tag{2}$$

Eq. (2), in which terms $r_{\alpha i}$ are the direction cosines, employs the Einstein's summation rule. Within the Cartesian reference system, it is possible to represent a direction corresponding to an elastically significant distortion as a point on the unit sphere (unit vector **a**), using two angles, θ (0,π) and φ (0,2π):

$$\mathbf{a} = \begin{pmatrix} \sin\theta\cos\varphi \\ \sin\theta\sin\varphi \\ \cos\theta \end{pmatrix} \tag{3}$$

For the calculation of the Young's modulus (E) or the linear compressibility (β), this single vector is sufficient. However, for shear modulus (μ) and the Poisson's ratio (ν), it is necessary to define a second vector **b**, placed perpendicularly to **a**. The second vector is characterized by a third angle, χ (0,2π), and by the coordinates:

$$\mathbf{b} = \begin{pmatrix} \cos\theta\cos\varphi\cos\chi - \sin\theta\sin\chi \\ \cos\theta\sin\varphi\cos\chi - \cos\theta\sin\chi \\ -\sin\theta\cos\chi \end{pmatrix} \tag{4}$$

Then, the coordinates of **a** and **b** represents the first two columns of the rotation matrix, which allow the calculation of all the components in the subvectorial space defined by directions 1 and 2 [18]:

$$S'_{12} = S'_{1122} = a_i a_j b_k b_l S_{ijkl} \quad \text{and} \quad S'_{66} = S'_{1212} = a_i b_j a_k b_l S_{ijkl}$$

The directional dependence of the elastic modulus and linear compressibility are defined as:

$$E(\theta,\varphi) = \frac{1}{S'_{11}(\theta,\varphi)} = \frac{1}{a_i a_j b_k b_l S_{ijkl}} \tag{5}$$

$$\beta(\theta,\varphi) = S_{ijkl} a_i a_j \tag{6}$$

whereas shear modulus and Poisson's ratio directional variation are given by the following formulas:

$$\mu(\theta,\varphi,\chi) = \frac{1}{4S'_{66}(\theta,\varphi,\chi)} \tag{7}$$

$$\nu(\theta,\varphi,\chi) = -\frac{S'_{12}(\theta,\varphi,\chi)}{S'_{11}(\theta,\varphi)} = \frac{a_i a_j b_k b_l S_{ijkl}}{a_i a_j a_k a_l S_{ijkl}} \tag{8}$$

Wave velocities were calculated by solving the Christoffel's equation.

Acknowledgments

The authors wish to thank the University of Bologna, Italy for funding the research.

Transparency document. Supporting information

Transparency data associated with this article can be found in the online version at https://doi.org/10.1016/j.dib.2018.10.139.

Appendix A. Supporting information

Supplementary data associated with this article can be found in the online version at https://doi.org/10.1016/j.dib.2018.10.139.

References

[1] G. Ulian, G. Valdrè, Equation of state and second-order elastic constants of portlandite $Ca(OH)_2$ and brucite $Mg(OH)_2$, Phys. Chem. Miner. (2018), https://doi.org/10.1007/s00269-018-0989-3 (In press).
[2] R. Dovesi, V.R. Saunders, C. Roetti, R. Orlando, C.M. Zicovich-Wilson, F. Pascale, B. Civalleri, K. Doll, N.M. Harrison, I.J. Bush, M. Llunell, M. Causà, Y. Noël, CRYSTAL14 User's Manual, University of Torino, Torino, 2014.
[3] R. Dovesi, V.R. Saunders, C. Roetti, R. Orlando, C.M. Zicovich-Wilson, F. Pascale, B. Civalleri, K. Doll, N.M. Harrison, I.J. Bush, P. D'Arco, M. Llunell, M. Causà, Y. Noel, L. Maschio, A. Erba, M. Rerat, S. Casassa, CRYSTAL17 User's Manual, University of Torino, Torino, 2017.
[4] G. Ulian, G. Valdrè, Dataset on the piezo-spectroscopic behaviour of hydroxylapatite: effect of mechanical stress on the Raman and Infrared vibrational bands from ab initio quantum mechanical simulations, Data Brief 18 (2018) 325–333.
[5] D. Moro, G. Ulian, G. Valdrè, Single molecule investigation of glycine-chlorite interaction by cross-correlated scanning probe microscopy and quantum mechanics simulations, Langmuir 31 (2015) 4453–4463.
[6] D. Moro, G. Ulian, G. Valdrè, Nanoscale cross-correlated AFM, Kelvin probe, elastic modulus and quantum mechanics investigation of clay mineral surfaces: the case of chlorite, Appl. Clay Sci. 131 (2016) 175–181.
[7] G. Ulian, G. Valdrè, Effect of mechanical stress on the Raman and infrared bands of hydroxylapatite: a quantum mechanical first principle investigation, J. Mech. Behav. Biomed. Mater. 77 (2018) 683–692.
[8] G. Ulian, G. Valdrè, M. Corno, P. Ugliengo, DFT investigation of structural and vibrational properties of type B and mixed A-B carbonated hydroxylapatite, Am. Miner. 99 (2014) 117–127.
[9] F. Peccati, M. Corno, M. Delle Piane, G. Ulian, P. Ugliengo, G. Valdrè, CO_3^{2-} mobility in carbonate apatite as revealed by density functional modeling, J. Phys. Chem. C 118 (2014) 1364–1369.
[10] A. Schafer, H. Horn, R. Ahlrichs, Fully optimized contracted Gaussian-basis sets for atoms Li to Kr, J. Chem. Phys. 97 (1992) 2571–2577.
[11] A.D. Becke, A new mixing of Hartree–Fock and local density-functional theories, J. Chem. Phys. 98 (1993) 1372–1377.
[12] C.T. Lee, W.T. Yang, R.G. Parr, Development of the Colle-Salvetti correlation-energy formula into a functional of the electron density, Phys. Rev. B 37 (1988) 785–789.
[13] M. Prencipe, F. Pascale, C.M. Zicovich-Wilson, V.R. Saunders, R. Orlando, R. Dovesi, The vibrational spectrum of calcite ($CaCO_3$): an ab initio quantum-mechanical calculation, Phys. Chem. Miner. 31 (2004) 559–564.
[14] S. Grimme, Semiempirical GGA-type density functional constructed with a long-range dispersion correction, J. Comput. Chem. 27 (2006) 1787–1799.
[15] G. Ulian, S. Tosoni, G. Valdrè, Comparison between Gaussian-type orbitals and plane wave ab initio density functional theory modeling of layer silicates: talc [$Mg_3Si_4O_{10}(OH)_2$] as model system, J. Chem. Phys. 139 (2013).
[16] G. Ulian, G. Valdrè, Density functional investigation of the thermo-physical and thermo-chemical properties of 2M1 muscovite, Am. Miner. 100 (2015) 935–944.
[17] G. Ulian, G. Valdrè, Structural, vibrational and thermophysical properties of pyrophyllite by semi-empirical density functional modelling, Phys. Chem. Miner. 42 (2015) 609–627.
[18] A. Marmier, Z.A.D. Lethbridge, R.I. Walton, C.W. Smith, S.C. Parker, K.E. Evans, ElAM: a computer program for the analysis and representation of anisotropic elastic properties, Comput. Phys. Commun. 181 (2010) 2102–2115.